Solid Freeform Fabrication 2023: Proceedings of the 34th Annual International Solid Freeform Fabrication Symposium – An Additive Manufacturing Conference
Reviewed Paper

Robot-aided selective embedding of a spatially steered fiber in polymer composite parts made using vat photopolymerization

Vivek Khatua*, B. Gurumoorthy*†, G. K. Ananthasuresh†

*Centre for Product Design and Manufacturing, Indian Institute of Science, Karnataka, India 560012
†Department of Mechanical Engineering, Indian Institute of Science, Karnataka, India 560012

Abstract

Fiber-Reinforced Polymer Composite (FRPC) parts are predominantly laminates, shells, or surfaces wound with 2+D fiber patterns even after the emergence of additive manufacturing. Making FRPC parts with embedded continuous fibers in 3D is not reported previously even though topology optimization demonstrates that such designs are optimal. Earlier attempts in 3D fiber reinforcement include making parts with channels into which fibers are inserted or co-extruding fiber with resin. In this work, A Vat-Photopolymerization Machine, and a process for concurrent embedding of spatially steered continuous fibers inside the matrix is developed. A single continuous fiber was embedded spatially using a robot to gradually steer the fiber as the part is built layer upon layer. An example of a fiber embedded along a helix in a cylindrical matrix is included in this work. Furthermore, a hinge effect was demonstrated when a fiber was embedded at a place that has substantial bending about the axis of the fiber.

1. Introduction

Continuous Fiber-Reinforced Polymer Composites (FRPCs) are stiff and strong due to the polymer matrix transferring loads to the fibers of high stiffness modulus. The fibers used in these FRPCs have high strength and stiffness modulus only in one direction (i.e., in tensile direction of the continuous fibers). Since their strength in one direction is highest, it is desired that the loads are transferred only in this direction. Hence, the paths in which the fibers are placed are crucial. In literature, continuous fibers are placed or embedded in a plane or on a surface. These surface-level placement and orientation are achieved by the state-of-the-art technologies in composite manufacturing, e.g., tailored fiber placement [1,2], open reed weaving [3,4] and robotic filament winding [5-7] and, additive manufacturing of FRPCs using vat photopolymerization [8-10] and fused deposition modelling [11-13]. However, fiber paths that are in 3D and embedded deep inside the matrix are seldom explored other than a few attempts that manually placed fibers in the interior of the part [12]. Fiber-reinforced composite structures with fibers deeply embedded in matrix are of interest as topology optimized structures with continuous fiber reinforcement show such intricate embedded fiber paths [14]. In this work, a 3D printing process was demonstrated, and a 3D printer is presented to embed a fiber path inside polymer matrix, which are difficult to manufacture using existing manufacturing techniques mentioned above. A hinge effect is demonstrated due to the inclusion of fibers in the structure at locations that undergo bending rather than elongation. We discuss the potential application of this hinge effect in making compliant mechanisms using fiber reinforcement.

2. Process and Method

2.1. Vat Photopolymerization Machine

The 3D printer developed is this work is a variant of Vat Photopolymerization (VP) machine to embed multiple *continuous* fibers that can continue along the build direction. Such an ability is enabled by eliminating a recoating blade from VP machines. A four degree-of-freedom serial robot arm situated above the vat positions, manipulates, orients, and steers the continuous fiber in each layer of the 3D printing process. Since a recoating blade is removed from the VP machine, a dip-coating method was adopted for recoating the cured surface. The initial layer of resin is manually spread across the build platform. Using this setup, a continuous fiber can be embedded along a given path that is a mathematical function parametrized along the build direction as there is no sweeping re-coater. Therefore, curves that cannot be represented as a function along the build-direction cannot be printed. Figure 1 shows the VP machine built for embedding fiber inside the matrix.

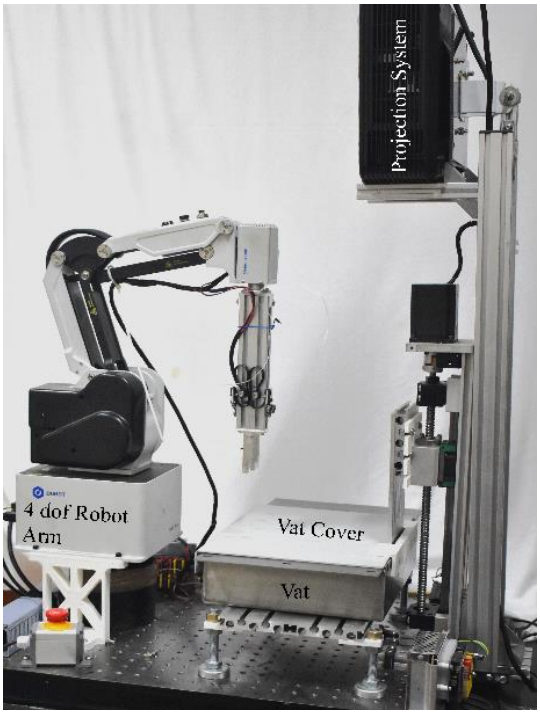

Figure 1 Vat photopolymerization machine developed for embedding continuous fibers along a spatial curve, the 4-dof robot arm enables gradual steering of fibers as the part is built layer upon layer.

2.2. 3D printing process

A.STL file is input for matrix domain of the composite part and the fiber data is fed as a piecewise continuous curve. This curve is then interpolated to get positions of the fiber at each layer along with the tangent and then, the end-effector position is determined at every layer. The end-effector of the robot holds the fiber in tension along the tangent in each layer at every point of the curve. Further, the slices and end-effector positions at each layer are fed to the 3D printer. The algorithm of the machine starts by projecting a black screen and then lowers the build platform to the focal plane of the projection. The algorithm now counts for the number of slices, finds slices where fibers needs to be steered and arranges the slices in an ordered list. Now, the projector iteratively projects images (from slices) along with the robot steering the fiber at every projection till the end of the list. At the end of the process, the fibers are manually cut. Figure 2 shows the flowchart of the process mentioned above.

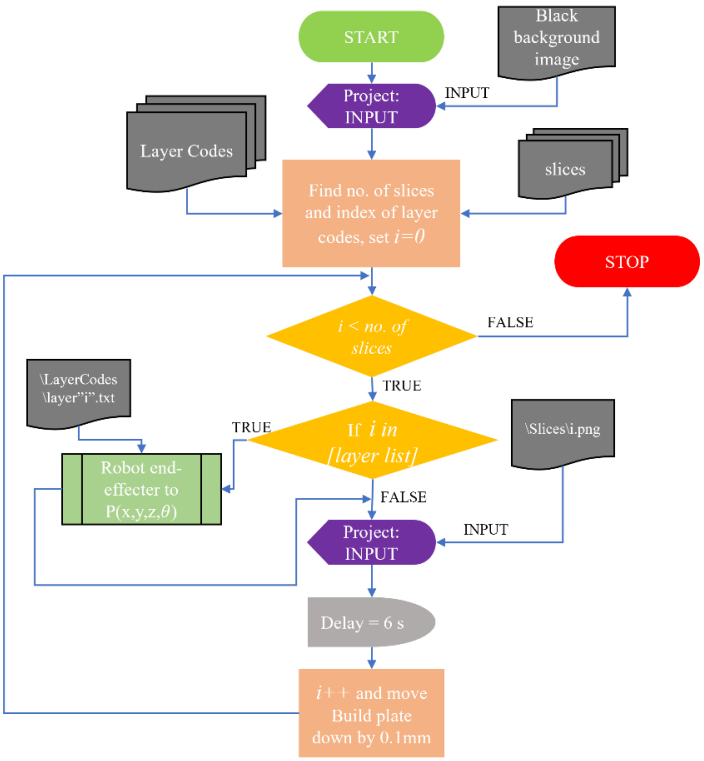

Figure 2 Flowchart of the 3D printing process for gradual steering of fibers

2.3. Materials

The photo-resin for the work is procured from Siraya Tech and mixed with Anycubic Clear in a ratio of 1:6 respectively. Both the resins have photo-initiators sensitive to 365 nm to 405 nm wavelength of light as claimed by the Manufacturers. The carbon-fiber tow used are provided by Marktech Pvt. Ltd., manufactured by Toray. The dry carbon fibers have a tensile modulus of 230 GPa and a tensile strength of 3.53 GPa as claimed by the manufacturer.

3. Results

3.1. Continuous fiber embedded along a helical path

An example of a fiber embedded along a helical path inside a cylindrical matrix domain is considered for the illustrating spatial fiber reinforcement embedded inside matrix. The parametric equation of a helix is reparametrized along the z direction to get the position of fiber at every layer and its corresponding tangents. Since the build platform moves down after every layer, the helical path of the fiber also moves down. The focal plane at $Z = 0$ is taken as the reference plane. The position of fiber at every layer is the projection of the curve on to the focal plane of the projector. The helix parametrized along the z direction $c(z)$ and the planar position of the curve at every layer $c_p(z)$ is as follows:

$$c(z) = \left(R\cos\frac{2\pi}{H}z, R\sin\frac{2\pi}{H}z, z\right) \quad (1)$$

$$c_p(z) = \left(R\cos\frac{2\pi}{H}z, R\sin\frac{2\pi}{H}z, 0\right) \quad (2)$$

The fiber is held by the robot at a constant length l along the tangent, away from the resin surface at every layer. The equation of the unit tangent $e_1(z)$ to $c(z)$ and the locus of end-effector $\vec{T}$ are as follows:

$$e_1(z) = \frac{dc/dz}{||dc/dz||} = \frac{2\pi R}{\sqrt{(2\pi R)^2 + H^2}}\left(-sin\frac{2\pi}{H}z, cos\frac{2\pi}{H}z, 1\right) \quad (3)$$

$$\vec{T} = le_1 + c_1(z) \quad (4)$$

Figure 3 shows helices with different helix angles embedded inside a cylindrical matrix. The fibers aligned along the tangent at every layer (as discussed previously) cast shadows. They result in an uncured region exposing the fiber track. These shadows are mitigated by moving the fiber at every layer after they are securely embedded on to the current layer. By doing so, the projector now exposes the regions that were in the shadow of the fiber. Figure 3b shows the shadow mitigated by employing such a method. After the parts are printed, they undergo post-curing in a heated UV chamber for a prolonged exposure of 30-40 mins.

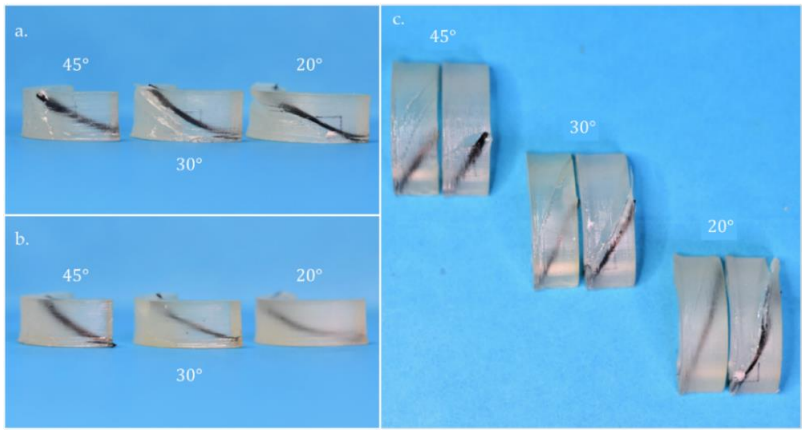

Figure 3 a shows fiber along helices that are made without mitigation for shadows, an uncured region can be noticed. b shows part printed by mitigating shadows of the fibers. c shows a side-by-side comparison of the effect of mitigating shadows

3.2. Hinge effect

A shallow circular arch with fiber embedded normal to the plane of the arch was considered to demonstrate a hinge effect. Fibers were embedded at different locations to understand the effect of embedding fibers where fiber does not participate in stretching, bending or compression. Flexibility to bending was found and this was due to the fibers placed at the vicinity of loading and boundary condition. The fiber in between loading and anchor points stiffens the structure. Figure 4 shows an illustration of an arch with fibers at three locations, viz. at the region of loading, near fixed conditions and in between boundary and loading condition. Fibers were

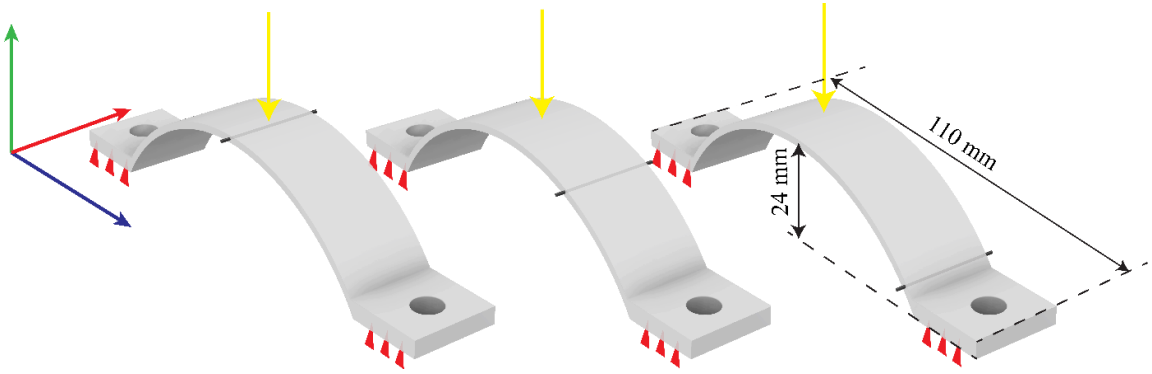

Figure 4 Shows three arches with fiber embedded at different locations, viz., at the region of loading (Left), at a region randomly in between loading and anchor points, and near anchor point (Right).

embedded as illustrated in Figure 4 and comparison was made with a similar part without fibers to verify the hinge effect. Upon compression of these arches, the arch without fiber is stiffer than the arch with fiber embedded at the location of loading. The parts with fiber embedded other than the site of loading make the arch stiffer. Figure 5 shows the phenomenon of a hinge with rotational stiffness seen in the linear elastic regime. A hinge with rotational stiffness can be observed in the part with fiber in the middle and in between loading and boundary condition by looking at the deformation in them. The rotational stiffness due to the fiber placed in between the loading point and constraints is the highest among all. Figure 6 shows the deformation patterns along with an exaggerated illustration of the deformed arches.

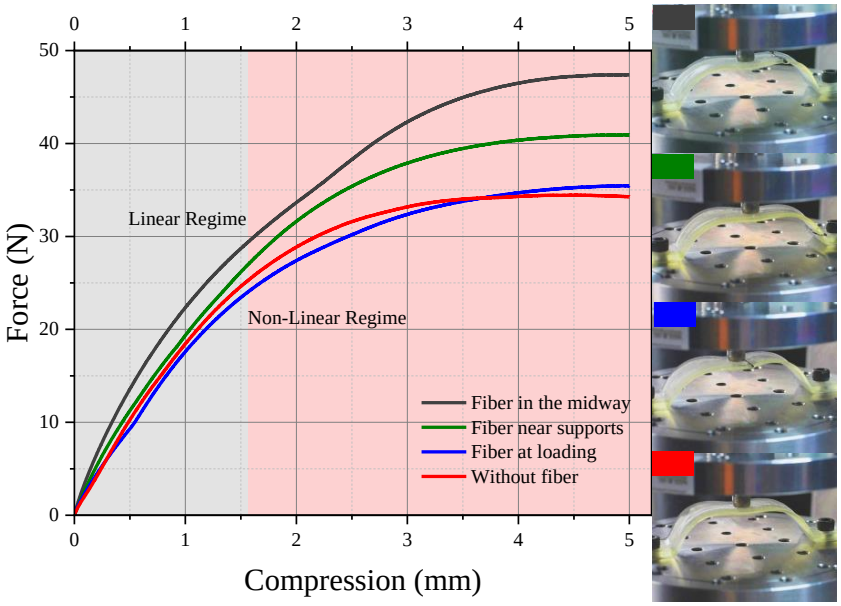

Figure 5 Force vs displacement graph of circular arches compared with an arch without fibers, the images in the right are indicated with colors corresponding to the force-displacement curves.

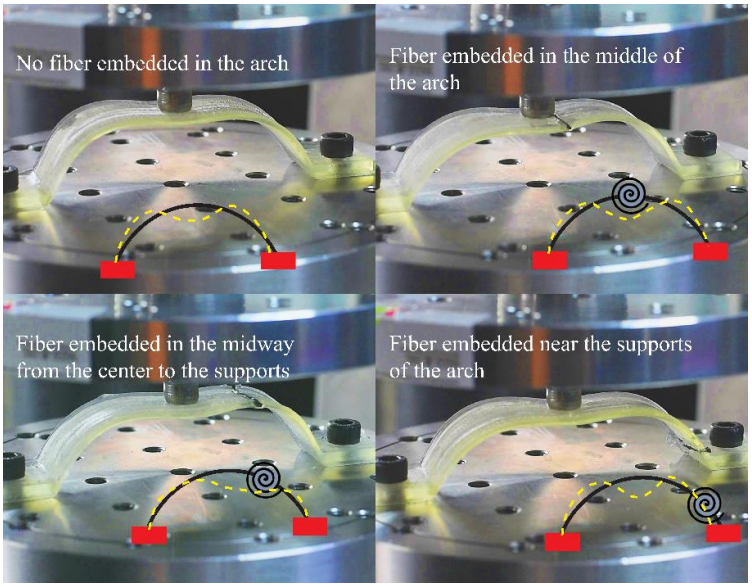

Figure 6 Shows the deformation of the arches due to the inclusion of fiber at different location of the arches. Illustrations in the figure show an exaggerated deformation pattern of the arches.

3.3. A compliant mechanism with fiber as a hinge

The hinge effect discussed previously was implemented in making a compliant mechanism with a rotational stiffness due to fiber reinforcement. A direction changing compliant mechanism with fibers embedded in the normal to the plane of deformation is made to illustrate the implementation. The compliant mechanism with fibers is found to be less stiff than the complaint mechanism without fibers whereas both are stiffer than the discrete compliant mechanism having flexural hinges. However, flexural hinges are known to break due to plastic deformation of the hinges. Figure 7 shows three compliant mechanisms used in this comparison. Figure 8 shows the force-displacement graph of these three mechanisms, the compliant mechanism with fiber shows a hinge effect as the stiffness is lower compared to the same mechanism without fiber.

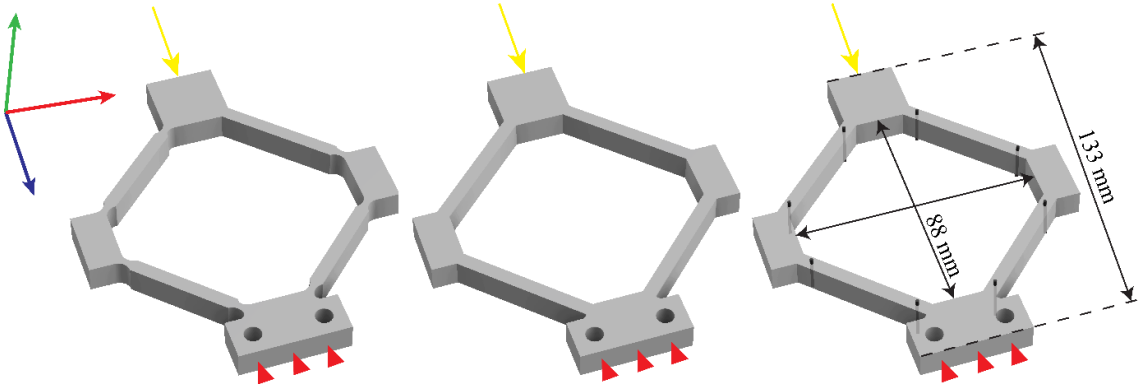

Figure 7 shows three compliant mechanisms with compression loading at the top and fixed supports in the bottom, the mechanism translates compression in one direction to extension in an orthogonal direction.

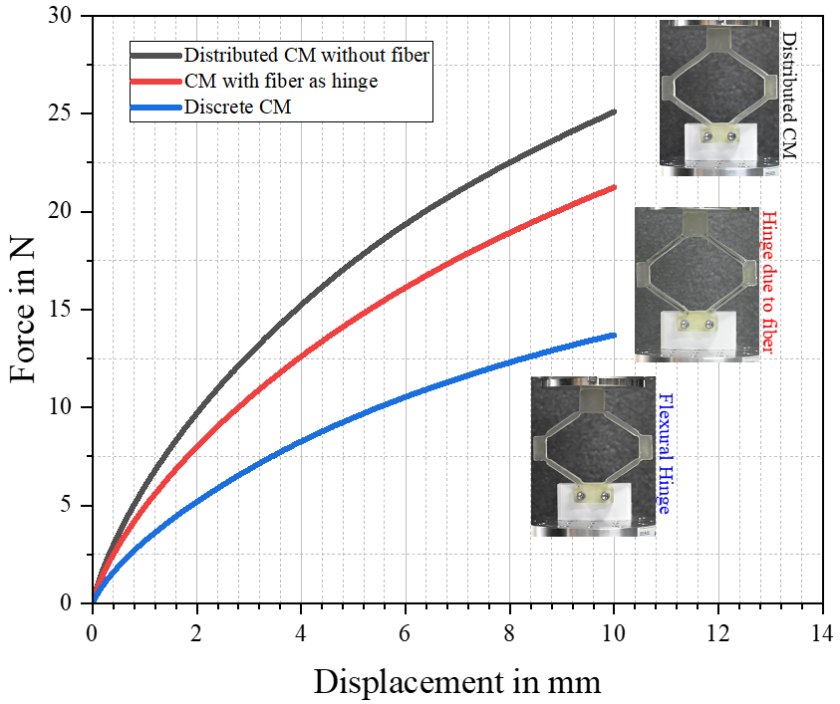

Figure 8 Force -Displacement graph of the compliant mechanisms under compression, an evident decrease in stiffness is seen due to the inclusion of fibers normal to the plane of deformation of the mechanism.

4. Closure

In the current work, the VP machine for embedding continuous fiber in spatial orientation was presented along with the 3D printing process. Although fiber steering capability was demonstrated, currently only a single continuous fiber can be steered. Multiple fibers can be embedded in a 3D part by either sequentially manufacturing segments of the whole part or implementing multiple robots embedding fibers in tandem. Each segment in sequential manufacturing may contain only one fiber that can be actively steered, and these segments join in the 3D printing process. The dip-coating method adopted was implemented for the resin used in this study. The time of print, coating thickness and surface finish may vary with different resin viscosities and surface tension of the resin. A counterintuitive phenomenon was observed when fibers are placed normal to the plane of deformation at the location of bending. Such inclusion of fibers in design and manufacturing of compliant mechanisms opens new possibilities for flexible yet strong hinges. However, further microscopical images are required to capture characteristics of the resin-fiber interface to provide insights into the hinge effect.

References

1. Takezawa, M., Otoguro, Y., Matsuo, K., Shibutani, T., Sakurai, A., & Maekawa, T. (2021). Fabrication of doubly-curved CFRP shell structures with control over fiber directions. *Computer-Aided Design*, *136*, 103028. https://doi.org/10.1016/j.cad.2021.103028
2. Uhlig, K., Spickenheuer, A., Bittrich, L., & Heinrich, G. (2013). *DEVELOPMENT OF A HIGHLY STRESSED BLADED ROTOR MADE OF A CFRP USING THE TAILORED FIBER PLACEMENT TECHNOLOGY* (Vol. 49, Issue 2).
3. Khan, S., Fayazbakhsh, K., Fawaz, Z., & Arian Nik, M. (2018). Curvilinear variable stiffness 3D printing technology for improved open-hole tensile strength. *Additive Manufacturing*, *24*, 378–385. https://doi.org/10.1016/J.ADDMA.2018.10.013
4. Ashir, M., Nocke, A., & Cherif, C. (2020). Adaptive fiber-reinforced plastics based on open reed weaving and tailored fiber placement technology. *Textile Research Journal*, *90*(9–10), 981–990. https://doi.org/10.1177/0040517519884578
5. Sorrentino, L., Marchetti, M., Bellini, C., Delfini, A., & del Sette, F. (2017). Manufacture of high performance isogrid structure by Robotic Filament Winding. *Composite Structures*, *164*, 43–50. https://doi.org/10.1016/j.compstruct.2016.12.061
6. Bodea, S., Zechmeister, C., Dambrosio, N., Dörstelmann, M., & Menges, A. (2021). Robotic coreless filament winding for hyperboloid tubular composite components in construction. *Automation in Construction*, *126*, 103649. https://doi.org/10.1016/j.autcon.2021.103649
7. Prado, M., Dörstelmann, M., Schwinn, T., Menges, A., & Knippers, J. (2014). Core-Less Filament Winding. In *Robotic Fabrication in Architecture, Art and Design 2014* (pp. 275–289). Springer International Publishing. https://doi.org/10.1007/978-3-319-04663-1_19
8. Lu, Y., Han, X., Gleadall, A., Chen, F., Zhu, W., & Zhao, L. (2022). Continuous fibre reinforced Vat photopolymerisation (CONFIB-VAT). *Additive Manufacturing*, *60*, 103233. https://doi.org/10.1016/J.ADDMA.2022.103233
9. Gupta, A., & Ogale, A. A. (2002). Dual curing of carbon fiber reinforced photoresins for rapid prototyping. *Polymer Composites*, *23*(6), 1162–1170. https://doi.org/10.1002/PC.10509
10. Renault, T., Ogale, A., & R, C. (n.d.). Selective reinforcement of photoresins with continuous fibers using 3-D composite photolithography. *Pascal-Francis.Inist.Fr*. Retrieved October 21, 2022, from https://pascal-francis.inist.fr/vibad/index.php?action=getRecordDetail&idt=3222781
11. Chen, X., Fang, G., Liao, W. H., & Wang, C. C. L. (2022). Field-Based Toolpath Generation for 3D Printing Continuous Fibre Reinforced Thermoplastic Composites. *Additive Manufacturing*, *49*, 102470. https://doi.org/10.1016/J.ADDMA.2021.102470
12. Brooks, H., & Molony, S. (2016). Design and evaluation of additively manufactured parts with three dimensional continuous fibre reinforcement. *Materials & Design*, *90*, 276–283. https://doi.org/10.1016/j.matdes.2015.10.123
13. Fernandes, R. R., van de Werken, N., Koirala, P., Yap, T., Tamijani, A. Y., & Tehrani, M. (2021). Experimental investigation of additively manufactured continuous fiber reinforced composite parts with optimized topology and fiber paths. *Additive Manufacturing*, *44*, 102056. https://doi.org/10.1016/j.addma.2021.102056

14. Jung, T., Lee, J., Nomura, T., & Dede, E. M. (2022). Inverse design of three-dimensional fiber reinforced composites with spatially-varying fiber size and orientation using multiscale topology optimization. *Composite Structures*, *279*. https://doi.org/10.1016/j.compstruct.2021.114768